Plasmonic-hot-electron mediated room-temperature generation of charged biexciton in monolayer WS_2

Zhiwei Peng, Tsz Wing Lo, and Dangyuan Lei*
Department of Materials Science and Engineering, City University of Hong Kong, Hong Kong 999077, China

(Received 17 December 2022; revised 3 March 2023; accepted 17 April 2023; published 9 May 2023)

Transition-metal dichalcogenide (TMDC) monolayers exhibit strong many-body Coulomb interaction, which induces rich excitonic states, including neutral exciton, trion (charged exciton), biexciton, and even charged biexciton. Despite the fact that the biexcitons in pristine two-dimensional (2D) TMDCs have great potential in forming correlated exciton pairs at distinct valleys, they lack efficient emission and optical tunability at room temperature, hindering their applications in photonic and optoelectronic devices. Here, we report room-temperature strong emission of the charged biexcitons from a gold nanosphere capped WS_2 monolayer through localized surface plasmon (LSP) induced hot-electron injection, and demonstrate all-optical control of the emission intensity through on- or off-resonant LSP excitation. Under on-resonant LSP excitation at 2.08 eV, the photoluminescence (PL) intensity shows a superlinear scaling with the laser power density, signifying the existence of charged biexcitons; On the contrary, the off-resonant LSP excitation at 2.33 eV results in no detectable PL signal of the charged biexcitons. By calculating the energy difference between the charged biexciton and trion, we further determine the binding energy of the former to be 25 meV. Our findings offer an opportunity for understanding the many-body effect associated with the charged biexcitons of 2D TMDCs, and could facilitate their potential quantum and optoelectronic applications under ambient environment.

DOI: 10.1103/PhysRevMaterials.7.054002

I. INTRODUCTION

The reduced dielectric screening in transition-metal dichalcogenides (TMDCs) monolayers enhances the Coulomb interaction between photoinduced electrons and holes. This results in the formation of various excitonic states (neutral excitons, trions, biexcitons, and charged biexcitons, etc.), which all have binding energies much larger than their bulk counterparts and hence dominate the optical properties of the materials even at elevated temperatures [1]. In particular, the direct band gap nature of the TMDCs at the monolayer limit further guarantees a strong valley-polarized excitonic photoluminescence (PL) at room temperature [2]. To utilize these intriguing excitonic properties of TMDCs monolayer for future optoelectronic and photonic device applications, external stimuli such as electric field [3–5], magnetic field [6–8], strain [9], ultrafast pulse excitation [10,11], and surface plasmon modes [12,13] have been employed to manipulate the behaviors of valley excitons. Up to now, both of the steady-state optical properties and ultrafast dynamics of neutral excitons [2] and trions [14,15] in TMDCs have been widely investigated at both cryogenic and room temperatures. However, direct observation of biexciton emission is restricted at cryogenic temperature [5,16,17], not to mention room-temperature active manipulation of the biexcitons emission. This is mainly attributed to the small binding energy of TMDCs biexcitons in comparison with that of neutral excitons (23.9 meV vs 509 meV for WS_2 monolayer) [18]. As a result, the enhanced exciton-phonon interaction at elevated temperatures easily promotes thermal dissociation of the biexcitons to form excitons. Since the TMDCs biexcitons provide a versatile low-dimensional platform for understanding the many-body effect and potential entanglement between pairs of valley pseudospins [19], there is an urgent need to develop an easy-to-implement method for brightening biexcitons and manipulating their properties at room temperature.

In this work, we demonstrate room-temperature formation and manipulation of charged biexcitons in monolayer WS_2 through the optically pumped injection of hot electrons from a single gold nanosphere (AuNS) coupling to the monolayer WS_2. Under on-resonant optical excitation, the nonradiative decay of localized surface plasmons (LSPs) in the AuNS supplies energetic electrons to the nearby WS_2 monolayer for promoting the formation of charged biexcitons to surpass the concurrent thermal dissociation rate. As a result, we observe that the PL spectral response of the WS_2-AuNS coupling system is dominated by charged biexcitons, which is further confirmed by the superlinear dependence of the integrated PL intensity on the excitation power density. Finally, comparing the energy difference between charged biexcitons and trions shows that the binding energy of the charged biexcitons in monolayer WS_2 is about 25 meV at room temperature.

II. RESULT AND DISCUSSION

WS_2 monolayers were mechanically exfoliated from a bulk single crystal using a Scotch tape method [20], and were subsequently transferred to a fused silica substrate

*dangylei@cityu.edu.hk

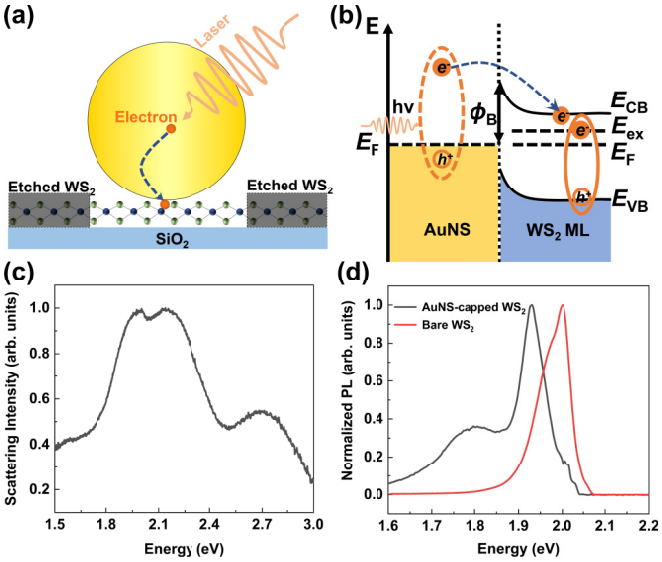

FIG. 1. Plasmonic-hot-electron injection modifies the electronic and optical properties of monolayer WS_2. (a) Schematic of LSP resonance-induced hot-electron injection from an AuNS to an underlying WS_2 monolayer. The WS_2 area underneath the AuNS remains intact after the RIE process, whereas the other area is etched. (b) Simplified energy diagram illustrating the hot-electron injection from the AuNS to the WS_2 monolayer, where E_{CB}, E_{VB}, E_F, and E_{ex} are the energies of conduction band, valance band, Fermi level and excitonic state, respectively. Under resonant excitation of the AuNS LSP mode, some conduction electrons in the AuNS are excited to energy levels well above E_F, and hence can overcome the Schottky barrier of the Au-WS_2 junction to reach the E_{CB} of WS_2, interacting with as-formed excitons to form new excitonic states such as trions and charged biexcitons. (c) Dark-field (DF) scattering spectrum of an AuNS above the WS_2 monolayer. (d) PL spectra of a bare WS_2 monolayer (red line) and our AuNS capped WS_2 monolayer (black line) both under 2.08 eV laser excitation.

through conventional all-dry viscoelastic stamping method [21]. AuNSs with an average diameter of 120 nm were dispersed onto both the WS_2 flakes and blank substrate through the drop casting method. The sample was subsequently etched for 5 s using an inductive coupled plasma etcher (TRION, Phantom RIE ICP) by argon plasma bombardment. The radio frequency power was 10 W at frequency of 13.56 MHz. The operational pressure was 10 mT, and 2 sccm flow rate of Ar gas was used to generate the plasma. The RIE process is used to minimize the PL contribution from the uncoupled WS_2 region, as illustrated in Fig. 1(a). Briefly, in the etching process, the AuNSs function as masks to protect the underlying WS_2 monolayer from being damaged by the argon ion gas to retain WS_2's pristine PL characteristics as seen from Fig. S1 in Supplemental Material [22]. In contrast, the PL response of the etched WS_2 monolayer is dominated by defect-bounded exciton emission while the band-edge PL is significantly suppressed. Note that in the coupling system, the AuNS serves as not only the etching mask to protect the WS_2 monolayer [23,24], but also a source of energetic electrons (hot electrons) under laser excitation [25,26]. To date, although the exact mechanism of LSP-induced hot-electron injection from metallic nanostructures to 2D semiconductors is still controversial [13,27–29], the hot-electron injection enabled modulations of neutral excitons [30,31] and optical band gap energy [32] in monolayer TMDCs have been achieved experimentally (yet at its true infancy stage). In this work, we utilize plasmonic hot-electron injection to realize room-temperature formation and all-optical manipulation of charged biexcitons in AuNS-coupled monolayer WS_2, which cannot be observed in pristine WS_2 under same excitation conditions.

A. On-resonant excitation

The WS_2-AuNS coupling system is sketched in Fig. 1(a), where the AuNS with a diameter of 120 nm is directly placed on the WS_2 monolayer (see its optical microscopy image in Fig. S2 [22]). The unshaded part of WS_2 represents the intact area protected from etching by the AuNS, and the shaded part is the etched area. Upon capping an AuNS on the WS_2 monolayer, a Schottky junction at the AuNS/WS_2 interface forms as illustrated in Fig. 1(b). When LSP resonance energy of plasmonic nanostructure such as AuNSs is larger than such Schottky barrier ϕ_B [33,34], the efficient injection of LSP-induced energetic electrons from the LSP band of AuNS to the monolayer WS_2 will be allowed. To investigate the modulation of excitonic states by the LSP-induced hot-electron injection, we first study the plasmonic properties of the AuNS in the etched-particle-on-WS_2-monolayer (EPoM) system. As seen from Fig. 1(c), the dark-field (DF) scattering spectrum of the EPoM system exhibits two peaks, with a Fano-like dip at 2.0 eV. By comparing this spectrum with the DF scattering spectra of an AuNS directly deposited on a bare SiO_2 substrate shown in Fig. S3(a) [22], we attribute the DF scattering spectral splitting to the considerable electrodynamic coupling between the transverse dipolar plasmon mode of the AuNS and the A excitons of the WS_2 monolayer [35,36]. The emerging small scattering peak at around 2.7 eV may originate from slight structural deformation of the AuNS induced in the RIE process since it is also observed in the DF scattering spectra of etched AuNSs on the bare SiO_2 substrate, as shown Fig. S3(b) [22]. Guided by the DF scattering spectra, we subsequently use a continuous wave (CW) laser of 2.08 eV to resonantly excite the dipolar plasmon mode of the AuNS, and the nonradiative decay of resonant LSPs provides hot electrons with energies above ϕ_B that can pass through the Schottky junction to reach the WS_2 monolayer and combine with as-formed excitons. To determine the possibility of sufficient plasmonic-hot-electron generation for exciton emission modulation by CW laser pumping on EPoM system, we perform the Mie theory calculation [37] to obtain the absorption cross section of the AuNS and estimate the time to produce a hot electron in Sec. D and Fig. S4 of Supplemental Material [22]. By comparing it with the exciton lifetime about 1 ns [38], we prove that hot-electron injection is sufficient in our system. As seen from Fig. 1(d), such hot-electron injection induces significant modification in the PL response of WS_2: the PL spectrum of the EPoM system exhibits a pronounced red shift in the dominant emission peak (up to 70 meV), and an additional emission peak originated from defect states in the etched WS_2 monolayer is also observed.

To further investigate the physical origin of the phenomenon observed in Fig. 1(d), we perform the excitation

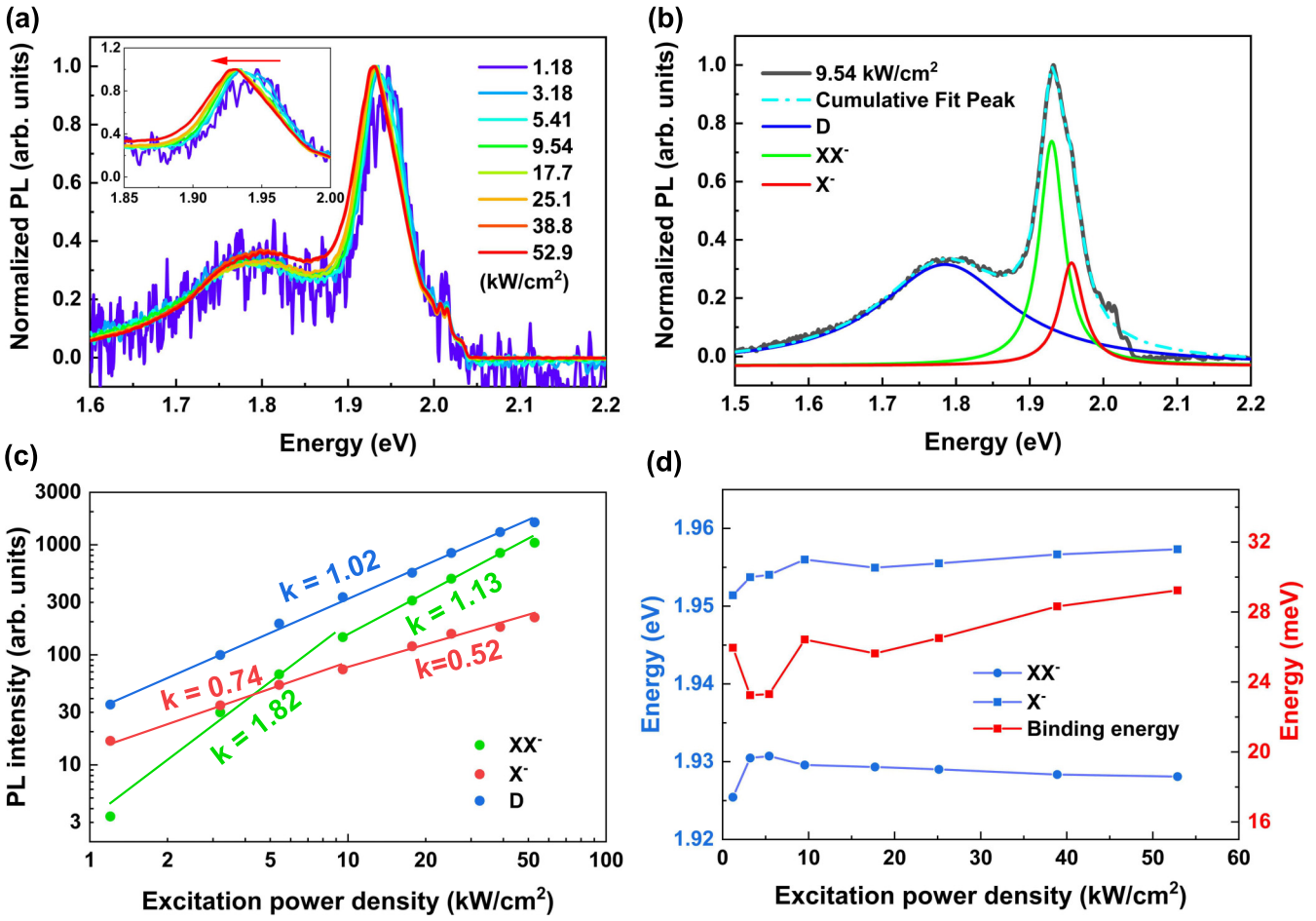

FIG. 2. The local injection of plasmonic hot electrons from the AuNS to the WS_2 monolayer triggers the formation of charged biexcitons at room temperature. (a) Power-dependent PL spectra of a EPoM system under 2.08 eV laser excitation. The inset shows a significant red shift in the highest peak when increasing the excitation power density. This represents the transition from trion to charged biexciton. (b) Spectral decomposition of PL from EPoM system taken at 9.54 kW/cm^2. The trion (X^-), charged biexciton (XX^-) and defect-bound exciton (D) are assigned. (c) Power-dependent integrated PL intensities of different excitons. At lower excitation laser power density, the XX^- emission intensity grows super-linearly with increasing excitation laser power density (giving an exponent of 1.82). In contrast, the X^- and D have exponents of 0.74 and 1.02, respectively. At higher excitation power densities, the exponents of both XX^- and X^- decrease sharply. (d) Power-dependent PL emission energies of XX^- and X^- extracted from (a) and corresponding binding energies of XX^- with respect to X^-.

power-dependent PL intensity measurements on the EPoM system, pure WS_2 monolayer, unetched single AuNS on WS_2 monolayer as seen in Fig. 2(a), Fig. S5, and Fig. S6 [22], respectively. Specifically, by comparing the PL spectra of the EPoM system and pure WS_2 monolayer at the high excitation power level, we verify the red shift of the dominant peak originated from the emergence of more complex excitonic states, namely, the charged biexciton. The spectra measured from EPoM system can be decomposed into three Lorentz peaks, the details of spectral line shape fitting are shown in Fig. S7 [22]. As shown in Fig. 2(b), we attribute those emission peaks to defect-bound exciton (D), charged biexciton (XX^-) [5,39], and charged exciton (trion, X^-), respectively. D probably originates from etched monolayer WS_2 region, while XX^- and X^- originate from the intact WS_2 monolayer region underneath the AuNS. In contrast, only two peaks emerge in the PL spectra of bare WS_2 monolayer where we attribute them to X^- and neutral exciton (X), respectively. The difference between the emission characteristic of the two systems is obvious. For the EPoM system, the excitons with net charge (both X^- and XX^-) dominate the spectra for almost all excitation power densities; however, the X^- and X are of comparable intensity even at much high excitation power density in the bare WS_2 monolayer. To investigate the physics mechanisms behind those abnormal excitonic states in the EPoM system, we plot the integrated PL intensity as a function of excitation laser power density in the double-logarithmic scale, as seen in Fig. 2(c). It is well known that the power-dependent proportionality relation of PL ($I \propto L^k$) indicates the characteristic features of the different excitons [39,40]. For the excitons in TMDCs monolayers, at low excitation power density, X and X^- usually are expected to exhibit linear dependence ($k = 1$) due to their excitonic transitions [5,41,42]. On the contrary, theoretically, the XX and XX^- will have the quadratic relationship ($k = 2$) between the PL intensity and excitation laser power density owing to the biexciton nature. However, in the real situation, the coefficients k of 1.2–1.9 are commonly observed for biexcitons owing to the inequivalent states [43,44]. In Fig. 2(c), when the excitation power level is low, the XX^-, D, X^- exhibit the superlinear,

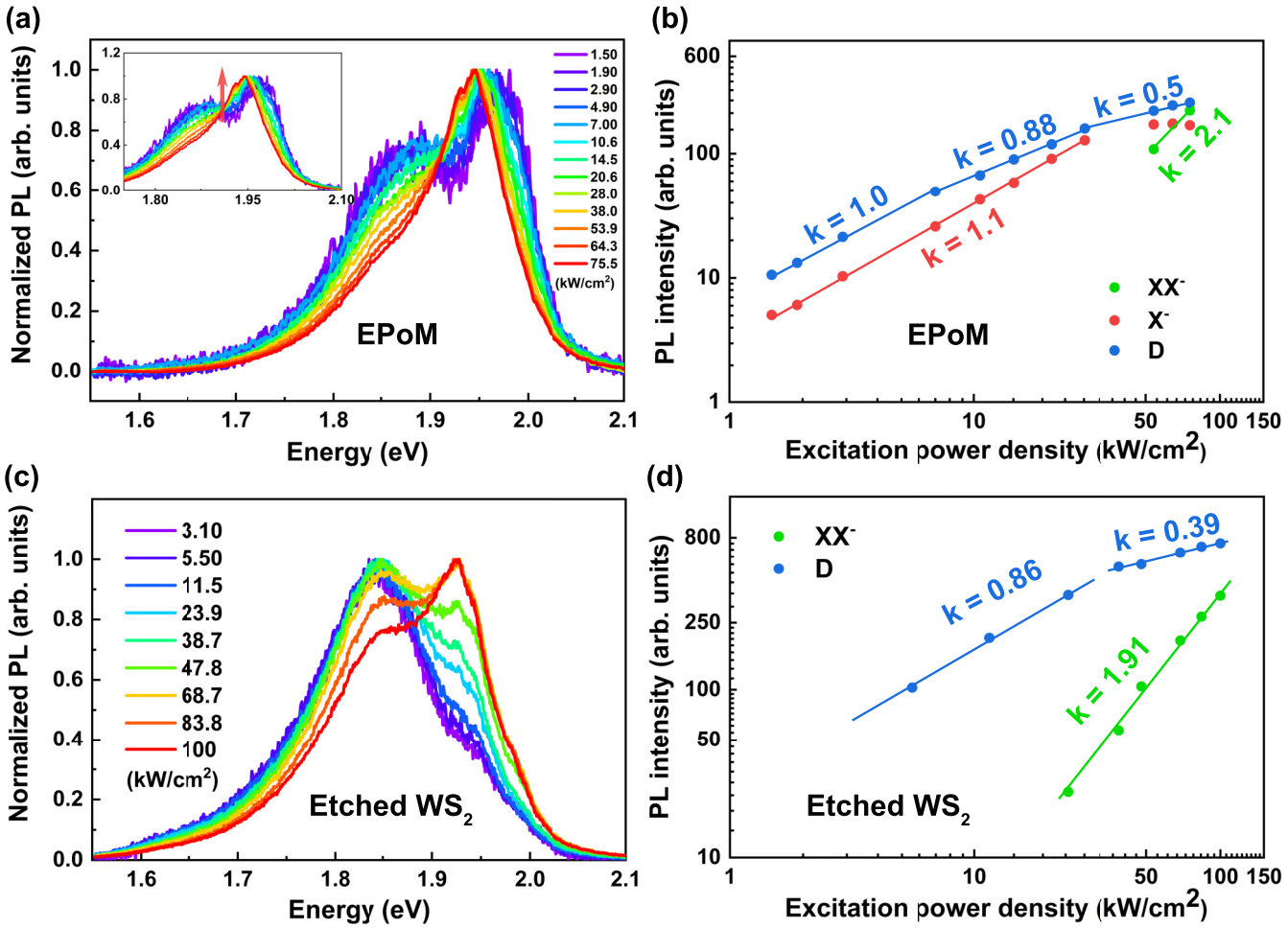

FIG. 3. PL spectra of the EPoM system under off-resonant LSP excitation condition. (a) Power-dependent PL spectra of the EPoM system under 2.33 eV laser excitation. The red arrow in the inset represents the appearance of the biexciton peak with increasing the excitation power density. (b) Power-dependent integrated PL intensities of different excitons of EPoM. The exponents of X^- and D are close to 1 but decrease sharply when the biexciton emission emerges, while the exponent $k = 2.1$ of XX^- shows its superlinear emission behavior. (c) Power-dependent PL characterizations of the etched WS_2 under 2.33 eV laser excitation. (d) Power-dependent PL integrated intensities of XX^- and D of etched WS_2. The exponents of D decrease quickly when the biexciton emerges.

linear, and sublinear relationship with the k of 1.82, 1.02, and 0.74, respectively. When the excitation power density is elevated to 10 kW/cm^2, the k of XX^- and X^- will reduce to 1.13 and 0.54, respectively, while the k of D does not change a lot. We attribute the decrease of k of XX^- and X^- at higher excitation power density to the saturation effect [45]. Moreover, we can infer that the threshold of excitation power density that can induce biexciton in our system is less than 1.18 kW/cm^2. As our results for the peak position and superlinear emission behavior of XX^- are consistent with the previous literature [5,42], we confirm that we do observe the charged biexciton channel dominant PL emission in the WS_2 monolayer at room temperature. The binding energy of charged biexciton with respect to X^- is defined as $E_b = E_{X^-} - E_{XX^-}$, where $E_{X^-}(E_{XX^-})$ are the energy of $X^-(XX^-)$ states determined by their emission energy displayed on the corresponding PL spectra [5]. The energy of X^-, XX^- and corresponding binding energy derived from the Fig. 2(a) are summarized in Fig. 2(d), representing that the binding energy of charged biexciton at room temperature is about 25 meV, which increases slightly with the increase of excitation power density and larger than the result under cryogenic temperature (21 meV at 4K) [5] due to the elevated temperature and electron density [46].

B. Off-resonant excitation

In order to confirm that the above-observed emission phenomenon of EPoM system originated from the plasmonic hot-electron injections, we switched the excitation laser from on-resonant energy (2.08 eV) of LSP mode to off-resonant energy (2.33 eV) of LSP mode for conducting the PL study. According to the DF scattering spectrum in Fig. 1(c), 2.33 eV is far away from the plasmon resonance of the AuNS. As a result, we expected that this control experiment involves negligible LSP-induced hot-electron injection and shows no obvious charged biexciton emissions. The power-dependent PL spectra in Fig. 3(a) show that, without plasmonic hot-electron injections, EPoM system does not show any charged biexciton emissions under relatively small excitation laser power density as we expected. As a result, the PL spectra are dominated by D and X^- in low excitation regime. Interestingly, when the excitation laser power density exceeds

40 kW/cm^2, we also observe the charged biexciton emission, as evidenced by the log-log plots in Fig. 3(b), in which we fitted two peaks (D and X^-) and three peaks (D, XX^-, and X^-) in lower (< 40 kW/cm^2) and higher (> 40 kW/cm^2) excitation power density region, respectively. The details of spectral line shape fitting and spectral decomposition of PL under different excitation laser power densities at off-resonant excitation can be find in Fig. S8 [22].

To investigate the physical origin of this unexpected biexciton emission in this off-resonant excitation of EPoM system, we perform the power-dependent PL measurements of the etched WS_2 monolayer region outside the coverage of AuNS, as shown in Figs. 3(c) and 3(d). The PL spectra under different excitation powers in Fig. 3(c) present that a new peak (around 1.93 eV) other than the D peak (approximately 1.83 eV) will appear when the excitation laser power density is larger than 20 kW/cm^2. The energy of this new peak (1.93 eV) is the same as that of XX^- observed in EPoM system [Fig. 3(a)], and its superlinear emission feature is evidenced in Fig. 3(d). Another noteworthy point is that when the excitation power is sufficiently high, XX^- emission dominates the PL emission and the D and X^- is suppressed simultaneously [Fig. 3(d)]. This suppressed D might originate from the competition of the defect centers in the WS_2 monolayer for forming D and XX^-. As we all know, for the intrinsic defect-free TMDCs monolayer, the PL is dominated by the neutral exciton emission. However, structural defects can induce unsaturated carriers, introducing doping effect to the TMDCs monolayer and forming charged excitonic states near the defects [47,48]. Defects in semiconductors generate intermediate states with energies that are smaller than the band gap. Even at low defect concentrations, those states can generate bound excitons that contribute significantly to the overall PL. The PL intensity of defect-bound excitons saturates at lower excitation power, while the free excitonic state (such as exciton and trion) show continuously filling with increasing excitation power [49,50]. However, in our case of high defect concentrations, the saturation power may be so large that the emission from free excitons become invisible. According to the above contents, we can conclude that the biexciton emission in the off-resonant excited EPoM system is dominated by the emission from the etched WS_2 monolayer. In contrast, the results are different in the case of on-resonant excited EPoM system, as shown in Fig. 2(c), where the k of D is nearly unchanged when we elevate the excitation power and observe XX^- emissions, which means there is no competition between the D and XX^-. It is believed that the LSP-induced hot-electrons injections to intact WS_2 monolayer support the additional charges for forming XX^- rather than the defect centers in the etched WS_2 monolayer. As a result, the competition relation between D and XX^- for defect centers is unnoticeable in the on-resonant excited EPoM system. This viewpoint is also verified by Fig. S1(a) [22], where the D peak dominates the PL of etched WS_2 monolayer under 2.08 eV, and XX^- is too weak to be observed even at a quite large excitation laser power density (252 kW/cm^2). Power-dependent PL measurements of the etched WS_2 monolayer region outside the coverage of AuNS are displayed on Fig. S9 [22] to support it.

From the above, although etched WS_2 can also generate the XX^- under off-resonant excitation, the generation of this XX^- from defect center is very inefficient and requires high excitation power density (the integrated XX^- PL intensity of the EPoM system at 50 kW/cm^2 excitation power density is about 1000 counts/s, while that of etched WS_2 monolayer is only 100 counts/s). In contrast, the XX^- generated by hot-electron injections in our EPoM system is much more efficient, and its threshold power density is less than 1.18 kW/cm^2.

III. CONCLUSION

In summary, we demonstrate efficient generation and modulation of charged biexciton emission in WS_2 monolayer at room temperature through plasmonic-hot-electron injections. This is a demonstration of the charged biexciton emission on mechanically exfoliated WS_2 monolayer at room temperature under such low laser excitation intensity. Quantitative analysis of the power-dependent PL spectra identifies its superlinear emission feature and determines the binding energy of charged biexciton at room temperature to be 25 meV. Our observation will deepen the understanding of the intrinsic properties of the various excitons in TMDCs monolayer and provide a platform for studying the many-body effect on the optical properties of 2D materials. On the other hand, the fabrication method we use can control the biexciton emission position, which may greatly benefit the potential applications in nanophotonics and biexciton lasing.

ACKNOWLEDGMENTS

We acknowledge financial support from the Research Grants Council of Hong Kong through the General Research Fund Grant No. (15304519). We thank Yancong Chen for careful proofreading and enlightening discussions.

[1] G. Wang, A. Chernikov, M. M. Glazov, T. F. Heinz, X. Marie, T. Amand, and B. Urbaszek, Rev. Mod. Phys. **90**, 021001 (2018).

[2] K. F. Mak, C. Lee, J. Hone, J. Shan, and T. F. Heinz, Phys. Rev. Lett. **105**, 136805 (2010).

[3] K. F. Mak, K. He, C. Lee, G. H. Lee, J. Hone, T. F. Heinz, and J. Shan, Nature Mater. **12**, 207 (2013).

[4] J. S. Ross, S. Wu, H. Yu, N. J. Ghimire, A. M. Jones, G. Aivazian, J. Yan, D. G. Mandrus, D. Xiao, W. Yao, and X. Xu, Nature Commun. **4**, 1474 (2013).

[5] Z. Ye, L. Waldecker, E. Y. Ma, D. Rhodes, A. Antony, B. Kim, X.-X. Zhang, M. Deng, Y. Jiang, Z. Lu *et al.*, Nature Commun. **9**, 3718 (2018).

[6] G. Aivazian, Z. Gong, A. M. Jones, R.-L. Chu, J. Yan, D. G. Mandrus, C. Zhang, D. Cobden, W. Yao, and X. Xu, Nature Phys. **11**, 148 (2015).

[7] Y. Li, J. Ludwig, T. Low, A. Chernikov, X. Cui, G. Arefe, Y. D. Kim, A. M. van der Zande, A. Rigosi, H. M. Hill, S. H. Kim, J. Hone, Z. Li, D. Smirnov, and T. F. Heinz, Phys. Rev. Lett. **113**, 266804 (2014).

[8] D. MacNeill, C. Heikes, K. F. Mak, Z. Anderson, A. Kormányos, V. Zólyomi, J. Park, and D. C. Ralph, Phys. Rev. Lett. **114**, 037401 (2015).

[9] Z. Peng, X. Chen, Y. Fan, D. J. Srolovitz, and D. Lei, Light Sci. Appl. **9**, 190 (2020).

[10] A. Chernikov, C. Ruppert, H. M. Hill, A. F. Rigosi, and T. F. Heinz, Nature Photon. **9**, 466 (2015).

[11] J. Kim, X. Hong, C. Jin, S.-F. Shi, C.-Y. S. Chang, M.-H. Chiu, L.-J. Li, and F. Wang, Science **346**, 1205 (2014).

[12] P. A. D. Gonçalves, L. P. Bertelsen, S. Xiao, and N. A. Mortensen, Phys. Rev. B **97**, 041402(R) (2018).

[13] X. Wen, W. Wang, X. Zhang, H. Chen, S. Jia, Y. Gong, W. Chen, Y. Wang, H. Zhu, J. Zheng *et al.*, Adv. Opt. Mater. **10**, 2100070 (2022).

[14] G. Wang, L. Bouet, D. Lagarde, M. Vidal, A. Balocchi, T. Amand, X. Marie, and B. Urbaszek, Phys. Rev. B **90**, 075413 (2014).

[15] T. Godde, D. Schmidt, J. Schmutzler, M. Aßmann, J. Debus, F. Withers, E. M. Alexeev, O. Del Pozo-Zamudio, O. V. Skrypka, K. S. Novoselov, M. Bayer, and A. I. Tartakovskii, Phys. Rev. B **94**, 165301 (2016).

[16] Y. You, X.-X. Zhang, T. C. Berkelbach, M. S. Hybertsen, D. R. Reichman, and T. F. Heinz, Nature Phys. **11**, 477 (2015).

[17] K. Hao, J. F. Specht, P. Nagler, L. Xu, K. Tran, A. Singh, C. K. Dass, C. Schüller, T. Korn, M. Richter *et al.*, Nature Commun. **8**, 15552 (2017).

[18] I. Kylänpää and H.-P. Komsa, Phys. Rev. B **92**, 205418 (2015).

[19] E. J. Sie, A. J. Frenzel, Y.-H. Lee, J. Kong, and N. Gedik, Phys. Rev. B **92**, 125417 (2015).

[20] K. S. Novoselov, A. K. Geim, S. V. Morozov, D. Jiang, Y. Zhang, S. V. Dubonos, I. V. Grigorieva, and A. A. Firsov, Science **306**, 666 (2004).

[21] A. Castellanos-Gomez, M. Buscema, R. Molenaar, V. Singh, L. Janssen, H. S. Van Der Zant, and G. A. Steele, 2D Mater. **1**, 011002 (2014).

[22] See Supplemental Material at http://link.aps.org/supplemental/10.1103/PhysRevMaterials.7.054002, which includes [37,38] for the detailed discussion of the hot electron injection efficiency. Furthermore, we provide the additional optical photos and spectra to support the viewpoints in the main text.

[23] Y. Jiang, H. Wang, S. Wen, H. Chen, and S. Deng, ACS Nano **14**, 13841 (2020).

[24] T. W. Lo, X. Chen, Z. Zhang, Q. Zhang, C. W. Leung, A. V. Zayats, and D. Lei, Nano Lett. **22**, 1915 (2022).

[25] Y. Kang, S. Najmaei, Z. Liu, Y. Bao, Y. Wang, X. Zhu, N. J. Halas, P. Nordlander, P. M. Ajayan, J. Lou *et al.*, Adv. Mater. **26**, 6467 (2014).

[26] M. L. Brongersma, N. J. Halas, and P. Nordlander, Nature Nanotechnol. **10**, 25 (2015).

[27] K. Wu, J. Chen, J. R. McBride, and T. Lian, Science **349**, 632 (2015).

[28] S. Tan, A. Argondizzo, J. Ren, L. Liu, J. Zhao, and H. Petek, Nature Photon. **11**, 806 (2017).

[29] M. W. Knight, H. Sobhani, P. Nordlander, and N. J. Halas, Science **332**, 702 (2011).

[30] K. R. Keller, R. Rojas-Aedo, H. Zhang, P. Schweizer, J. Allerbeck, D. Brida, D. Jariwala, and N. Maccaferri, ACS Photonics **9**, 2683 (2022).

[31] J. Ma, G.-B. Liu, and S. Gao, Phys. Rev. B **105**, 075434 (2022).

[32] Y.-H. Chen, R. R. Tamming, K. Chen, Z. Zhang, F. Liu, Y. Zhang, J. M. Hodgkiss, R. J. Blaikie, B. Ding, and M. Qiu, Nature Commun. **12**, 4332 (2021).

[33] C. Kim, I. Moon, D. Lee, M. S. Choi, F. Ahmed, S. Nam, Y. Cho, H.-J. Shin, S. Park, and W. J. Yoo, ACS Nano **11**, 1588 (2017).

[34] L.-X. Zhou, Y.-T. Ren, Y.-T. Chen, X.-H. Lv, C.-D. Jin, H. Zhang, P.-L. Gong, R.-Q. Lian, R.-N. Wang, J.-L. Wang *et al.*, Phys. Rev. B **105**, 224105 (2022).

[35] C. Carlson, R. Salzwedel, M. Selig, A. Knorr, and S. Hughes, Phys. Rev. B **104**, 125424 (2021).

[36] T. W. Lo, Q. Zhang, M. Qiu, X. Guo, Y. Meng, Y. Zhu, J. J. Xiao, W. Jin, C. W. Leung, and D. Lei, ACS Photonics **6**, 411 (2019).

[37] S. J. Oldenburg, Light Scattering from Gold Nanoshells, Ph.D. thesis, Rice University, Houston, 2000.

[38] M. Kulig, J. Zipfel, P. Nagler, S. Blanter, C. Schüller, T. Korn, N. Paradiso, M. M. Glazov, and A. Chernikov, Phys. Rev. Lett. **120**, 207401 (2018).

[39] S. Chatterjee, S. Das, G. Gupta, K. Watanabe, T. Taniguchi, and K. Majumdar, 2D Mater. **9**, 015023 (2021).

[40] T. Schmidt, K. Lischka, and W. Zulehner, Phys. Rev. B **45**, 8989 (1992).

[41] S.-Y. Chen, T. Goldstein, T. Taniguchi, K. Watanabe, and J. Yan, Nature Commun. **9**, 3717 (2018).

[42] I. Paradisanos, S. Germanis, N. Pelekanos, C. Fotakis, E. Kymakis, G. Kioseoglou, and E. Stratakis, Appl. Phys. Lett. **110**, 193102 (2017).

[43] R. T. Phillips, D. J. Lovering, G. J. Denton, and G. W. Smith, Phys. Rev. B **45**, 4308 (1992).

[44] M. Barbone, A. R.-P. Montblanch, D. M. Kara, C. Palacios-Berraquero, A. R. Cadore, D. De Fazio, B. Pingault, E. Mostaani, H. Li, B. Chen *et al.*, Nature Commun. **9**, 3721 (2018).

[45] J. Shang, X. Shen, C. Cong, N. Peimyoo, B. Cao, M. Eginligil, and T. Yu, ACS Nano **9**, 647 (2015).

[46] S. Golovynskyi, O. I. Datsenko, D. Dong, Y. Lin, I. Irfan, B. Li, D. Lin, and J. Qu, J. Phys. Chem. C **125**, 17806 (2021).

[47] H. Qiu, T. Xu, Z. Wang, W. Ren, H. Nan, Z. Ni, Q. Chen, S. Yuan, F. Miao, F. Song *et al.*, Nature Commun. **4**, 2642 (2013).

[48] S. Zhang, C.-G. Wang, M.-Y. Li, D. Huang, L.-J. Li, W. Ji, and S. Wu, Phys. Rev. Lett. **119**, 046101 (2017).

[49] S. Haldar, H. Vovusha, M. K. Yadav, O. Eriksson, and B. Sanyal, Phys. Rev. B **92**, 235408 (2015).

[50] J. Pandey and A. Soni, Appl. Surf. Sci. **463**, 52 (2019).